Ginsenoside Rg3 Induces Apoptosis and Inhibits Proliferation By Down-Regulating TIGAR in MNNG-Induced Gastric Precancerous Lesions in Rats

Shangbin Lv
Basic Medical College, Chengdu University of Traditional Chinese Medicine
Xiaodong Chen
Department of Surgery, Sichuan Cancer Hospital, School of Medicine, University of Electronic Science and Technology of China
Gang Mao
Hospital of Chengdu University of Traditional Chinese Medicine
Daoyin Gong
Hospital of Chengdu University of Traditional Chinese Medicine
Yu Chen
Hospital of Chengdu University of Traditional Chinese Medicine
Ting Xia
Hospital of Chengdu University of Traditional Chinese Medicine
Jing Cheng
Basic Medical College, Chengdu University of Traditional Chinese Medicine
Zhaoliang Luo
Basic Medical College, Chengdu University of Traditional Chinese Medicine
Yu Cheng
Basic Medical College, Chengdu University of Traditional Chinese Medicine
Jinhao Zeng (zengjinhao@cdutcm.edu.cn)
Department of Chinese Internal Medicine, Hospital of Chengdu University of Traditional Chinese Medicine
Weihong Li
Basic Medical College, Chengdu University of Traditional Chinese Medicine

---

Research Article

Keywords: Ginsenoside Rg3, gastric precancerous lesions, Apoptosis, TP53-induced glycolysis and apoptosis regulator, reactive oxygen species

Posted Date: December 9th, 2021

DOI: https://doi.org/10.21203/rs.3.rs-1099025/v1

Abstract

BACKGROUND

Ginsenoside Rg3 (GRg3) is one of the main active ingredients in Chinese ginseng extract and has various biological effects, such as immune-enhancing, antitumour, antiangiogenic, immunomodulatory and anti-inflammatory effects. This study aimed to investigate the therapeutic effect of GRg3 on gastric precancerous lesion (GPL) induced by N-methyl-N'-nitro-N-nitrosoguanidine (MNNG) and the potential mechanism of action.

METHODS

The MNNG–ammonia composite modelling method was used to establish a rat model of GPL. Histopathological changes in the rat gastric mucosa were observed by pathological analysis using haematoxylin–eosin staining to assess the success rate of the composite modelling method. Alcian blue–periodic acid Schiff staining was used to observe intestinal metaplasia in the rat gastric mucosa. Apoptosis was detected in rat gastric mucosal cells by terminal deoxynucleotidyl transferase-mediated dUTP nick end labelling staining. The expression level of reactive oxygen species (ROS) was determined by the dihydroethidium fluorescent probe method, and that of TP53-induced glycolysis and apoptosis regulator (TIGAR) protein was determined by immunohistochemical staining and western blotting. The expression levels of nicotinamide adenine dinucleotide phosphate (NADP) and glucose-6-phosphate dehydrogenase (G6PDH) were determined by an enzyme-linked immunosorbent assay, and that of glutathione (GSH) was determined by microanalysis.

RESULTS

GRg3 significantly alleviated the structural disorganization and cellular heteromorphism in the form of epithelial glands in the gastric mucosa of rats with GPL and retarded the progression of the disease. Overexpression of TIGAR, NADP, GSH and G6PDH occurred in the gastric mucosal epithelium of rats with GPL, which in turn led to an increase in the ROS concentration. After treatment with GRg3, the expression of TIGAR, NADP, GSH and G6PDH decreased, causing a further increase in the concentration of ROS in the gastric mucosal epithelium, which in turn induced apoptosis and played a role in inhibiting the abnormal proliferation and differentiation of gastric mucosal epithelial cells.

CONCLUSION

Grg3 can induce apoptosis and inhibit cell proliferation in MNNG-induced GPL rats. The mechanism may be related to down regulating the expression levels of TIGAR, GSH, NADP and G6PD, up regulating the concentration of ROS and inducing apoptosis.

1. Introduction

Gastric precancerous lesion (GPL) is usually classed as intestinal metaplasia (IM) or gastric epithelial dysplasia (DYS). GPL is closely associated with the pathogenesis of gastric cancer (GC). The latest data show that GC is the fifth most common cancer worldwide and the fourth leading cause of death among cancer patients worldwide [1]. Because there is a direct link between the development of GC and GPL, preventing the progression of GPL to GC is the key to reducing the incidence of GC [2]. Modern medicine does not have specific drugs for GPL, and endoscopic mucosal resection is only performed when a patient is diagnosed with severe gastroesophageal reflux disease and definite intramucosal cancer. However, most patients with GPL cannot undergo endoscopic resection, and modern medicine thus lacks effective interventions for GPL [3]. Therefore, the search for simple and effective alternative treatments has always been an important topic of research.

Ginsenoside Rg3 (GRg3) is one of the main active ingredients extracted from ginseng and has a wide range of pharmacological activities, including immune-enhancing, antitumour, antiangiogenic, immunomodulatory, anti-inflammatory and antioxidant effects [4–8]. GRg3 can also be used as an adjuvant for traditional cancer treatments to reduce their toxicity and increase their efficiency via its synergistic action [9].

Moreover, GRg3 has been shown to significantly inhibit tumour growth in different cancer models [10, 11]. Recent studies have shown that its activity is mainly associated with the induction of apoptosis, inhibition of proliferation and angiogenesis, regulation of immunity and inhibition of multidrug resistance, which increases chemosensitivity [12]. GRg3 has been found to be effective against GC in *in vivo* and *in vitro* studies and might be a promising agent for the treatment of GC. *In vitro* tests showed that GRg3 inhibited the activity of SGC-7901 cells by regulating the phosphatase and tensin homologue/p-phosphoinositide 3-kinase (PI3K)/Akt pathway [13]. Other tests showed that GRg3 inhibited the expression of hypoxia-inducible factor-1α and vascular endothelial growth factor in BGC823 human GC cells and thereby inhibited metastasis in GC [14]. Animal tests demonstrated that GRg3 inhibited neoangiogenesis and thereby suppressed tumour growth and metastasis in a severe combined immunodeficient mouse model of human GC [15]. GRg3 also inhibited fucosyltransferase-4-induced apoptosis in gastric mucosal cells by upregulating Sp1 and downregulating heat shock factor-1 [16]. In this study, we used a rat model of GPL to investigate the interventional effects and potential mechanisms of GRg3 on the gastric mucosa of rats with N-methyl-N'-nitro-N-nitrosoguanidine (MNNG)-induced GPL.

It is well known that tumours grow because of uncontrolled cell proliferation [17] and that reactive oxygen species (ROS) are closely associated with the proliferation of tumour cells. When the ROS concentration is maintained at a fairly high level, cells are in a state of oxidative stress that cannot be alleviated by antioxidants. This can damage intracellular DNA, proteins and organelles and thus lead to lethal cell damage and trigger apoptosis [18]. However, if the ROS concentration is increased to an appropriate, nonlethal level, cells will instead gradually adapt. This creates a new redox balance and enables

abnormal cell proliferation, which is associated with various processes such as tumour cell survival and proliferation, angiogenesis and metastasis [19, 20]. In rapidly proliferating cells, fluctuations in the expression of both glutathione (GSH), which protects cells and biological macromolecules such as proteins from damage due to ROS, and nicotinamide adenine dinucleotide phosphate (NADP), which maintains GSH in its reduced state, occur as a result of an increase in the expression of ROS [21]. Therefore, ROS have become an important subject of research from the perspective of cellular redox homoeostasis. TP53-induced glycolysis and apoptosis regulator (TIGAR) is a protein that regulates glucose-6-phosphate dehydrogenase (G6PDH), NADP and GSH, and an increase in its expression leads to abnormal activation of G6PDH, NADP and GSH [22], of which the intracellular concentrations are thus maintained at high levels. This makes the antioxidant system in cells relatively stable, and ROS concentrations can be maintained at relatively high levels that enable rapid cell proliferation without triggering apoptosis [23, 24]. In GC, after knockdown of TIGAR cells would be unable to scavenge ROS because insufficient amounts of NADP, G6PDH and GSH were synthesized, and cells would be in a state of oxidative stress that activated the apoptosis pathway and inhibited excessive proliferation of GC cells [25]. At present, however, there have been few studies of TIGAR in the GPL stage.

In this study, we investigated whether GRg3 can affect apoptosis and proliferation of gastric mucosal cells by regulating TIGAR, GSH, G6PDH and NADP. In order to elucidate the potential mechanism of the intervention of GRg3 in GPL, we found evidence that GRg3 can play a role in promoting repair of the gastric mucosa and retarding the progression of the disease by triggering apoptosis.

2. Materials And Methods

2.1 Animals

Seventy-four male Sprague-Dawley rats with weights of 190 ± 10 g and ages of 6–7 weeks were provided by Chengdu Dashuo Biotechnology Co., Ltd and were housed in a laboratory at Chengdu University of Traditional Chinese Medicine on a 12 h/12 h light/dark cycle. The room temperature was maintained at 20 ± 2 ℃, and the relative humidity was maintained at 50–70%. The animal experiments in this study were approved by the Experimental Animal Ethics Committee of Chengdu University of Traditional Chinese Medicine (audit filing number: 2019-17).

2.2 Establishment and treatment of rat model of GPL

A rat model of GPL was established by the MNNG–ammonia composite modelling method. MNNG was purchased from Tokyo Chemical Industry Company, Japan (item number: CFFC-M0527-5G). The modelling process is shown in Fig. 1. First, the 74 rats were divided into normal (n = 12) and model (n = 62) groups using the digital random table method. The rats in the normal group were housed routinely, and the rats in the model group were given an ammonia solution with a concentration of 0.1% and were allowed to drink freely. Ammonia was purchased from China Sichuan Kebei Biological Company Limited (item number: GB/T631-2007). The rats in the model group received a 200 μg mL^{-1} MNNG solution by

gavage and were fasted twice a week for 24 h each time without drinking [26]. At the end of week 8, two animals were randomly selected from the model group, from which the gastric mucosa at the gastric body–sinus junction was removed and stained with haematoxylin and eosin (H&E) to confirm the presence of early GPL in the form of mucosal intestinal epithelial metaplasia under light microscopy. The rats in the model group were then randomly divided into a model group, a folic acid group and high-, medium- and low-dose GRg3 groups, each of which comprised 12 rats. All groups except the normal group continued to receive the 0.1% ammonia solution *ad libitum* and the 200 μg mL^{-1} MNNG solution by gavage. Gavage treatment was started in week 9. The folic acid group received 2.7 mg kg^{-1} day^{-1} folic acid. Folic acid tablets were obtained from Changzhou Pharmaceutical Factory Co., Ltd (lot number: H32023302). The high-, medium- and low-dose GRg3 groups received 7.2 mg kg^{-1}, 3.6 mg kg^{-1} and 1.8 mg kg^{-1} GRg3, respectively. GRg3 was supplied by Hefei Bomei Biotechnology Co., Ltd (item number: BZP0239). The normal and model groups received 1 mL/100 g saline by gavage. The rats were treated by gavage for 12 weeks.

2.3 Pathological analysis

After being fasted for 12 h, the animals were euthanized with sodium pentobarbital (2 mL g^{-1}). The stomach was immediately removed, cut along the greater curvature and fixed in 4% paraformaldehyde fixative. Each sample was then embedded in paraffin and serially sectioned to a thickness of 3 μm. The sections were stained with H&E to observe histopathological changes in the gastric mucosa. In addition, the type of IM was determined using Alcian blue–periodic acid Schiff (AB-PAS) staining.

2.4 Terminal deoxynucleotidyl transferase dUTP nick end labelling staining

Paraffin sections (n = 10 per group) were dewaxed according to the instructions of a terminal deoxynucleotidyl transferase dUTP nick end labelling (TUNEL) staining kit (Servicebio, No. G1507). The sections were shaken gently until dry, and the tissue was then circled with a histochemical pen (Servicebio, No. WG1066-1). A working solution of proteinase K was added dropwise inside the circle to cover the tissue, which was incubated at 37°C for 20 min. The sections were placed in phosphate-buffered saline (PBS) (pH 7.4) and washed three times with shaking on a decolorizing shaker for 5 min each time. The sections were placed in a 3% hydrogen peroxide solution and incubated for 20 min at room temperature while protected from light. The slices were shaken gently until dry, and buffer was added dropwise to cover the tissue in the circle. The slices were then incubated at room temperature for 10 min. After that, the equilibration solution was removed, and recombinant terminal deoxynucleotidyl transferase, biotin–dUTP labelling mix and equilibration buffer were mixed in a ratio of 1 μL: 5 μL: 50 μL and added to the circle to cover the tissue. The sections were placed flat in a wet box and incubated at 37°C for 1 h. A small amount of water was added to the wet box to maintain the humidity. After that, the sections were placed in PBS (pH 7.4) on a decolorizing shaker and washed three times for 5 min each. Streptavidin–horseradish peroxidase (HRP) and Tris-buffered saline–Tween-20 (TBST) were incubated at 1:200. The sections were placed in PBS (pH 7.4) and washed three times for 5 min each time with

shaking on a decolorizing shaker. The sections were shaken gently, and freshly prepared 3,3'-diaminobenzidine (DAB) colour development solution (Servicebio, No. G1212) was added. The colour development time was controlled under a microscope, and the colour development was terminated by rinsing the sections with pure water. The sections were dehydrated in four cylinders of 100% alcohol for 5 min each time and were then immersed in *n*-butanol for 5 min, placed in xylene for more than 5 min until transparent, taken out to dry and sealed with neutral gum. Afterwards, the sealed slices were placed under a 200× high-magnification microscope. Five fields of view were randomly selected to count positively stained cells, and the apoptosis rate was calculated according to the following formula: apoptosis rate = number of positively stained cells/(number of positively stained cells + number of unstained cells) × 100%. Each set of data was measured three times, and the average value was taken. Brownish-yellow or brown granules in the nucleus were regarded as positive TUNEL staining.

2.5 Dihydroethidium fluorescent probe method

Frozen sections were warmed to room temperature while the humidity was controlled and were then dried. Circles were drawn around the tissue with a histochemical pen, and an autofluorescence quencher (Servicebio, No. G1221) was added for 5 min to the circles, which were then rinsed with running water for 10 min. An ROS staining solution (Sigma, D7008) was added dropwise to the circles, which were then incubated at 37°C for 30 min in a light-proof thermostatted box. The sections were placed in PBS (pH 7.4), shaken and washed three times for 5 min each time on a decolorizing shaker.. The sections were shaken, dried and sealed with an anti-fluorescence quenching sealer (Servicebio, No. G1401). The sections were observed under a fluorescence microscope, and images were collected with red fluorescence regarded as positive staining. 4',6-Diamidino-2-phenylindole: UV excitation wavelength 330–380 nm, emission wavelength 420 nm, blue light; fluorescein isothiocyanate: excitation wavelength 465–495 nm, emission wavelength 515–555 nm, green light; Cy3: excitation wavelength 510–560 nm, emission wavelength 590 nm, red light. The average absorbance values were calculated using ImageJ software.

2.6 Protein blotting

Gastric mucosal tissues (n = 10 per group) were homogenized and lysed in sample buffer, and then the lysates were centrifuged at 12000 rpm for 10 min at 4°C. The protein solution was then added to protein loading buffer in a ratio of 4:1, denatured in a boiling water bath for 15 min and stored in a freezer at −20°C as a backup. Equal amounts of protein from each sample were separated by 10% sodium dodecyl sulphate polyacrylamide gel electrophoresis and transferred to polyvinylidene difluoride membranes. The membranes were decolorized at room temperature on a shaker with 5% skimmed milk in a 0.5% TBST preparation and were then incubated with a diluted primary antibody (anti-TIGAR antibody; Abcam, ab189164) at 4°C overnight. A secondary antibody (HRP-labelled goat anti-rabbit; Servicebio, No. GB23303) was then added at room temperature, and the mixture was held for 1 h. The protein expression was assessed using an ultra-enhanced chemiluminescence reagent (K003; Affinity Biosciences, Cincinnati, OH, USA). β-Actin was used as an internal control, and the optical density (OD) of each band was determined using ImageJ software.

2.7 Biological data mining methodology

Clinical data on GC and data on TIGAR expression were downloaded from the Cancer Genome Atlas (TCGA) database and included data for 32 normal samples and 375 GC samples. To investigate the biological processes involved in low and high expression of TIGAR in GC, gene set enrichment analysis (GSEA) was performed on the transcriptomics data from the TCGA on GC, which included data on 19645 genes and 375 samples. The median value for the expression of TIGAR was used to classify these 375 samples into high- and low-expression groups, and GSEA software was used for analysis.

2.8 Immunohistochemical staining

Gastric tissue sections were fixed in 4% paraformaldehyde at room temperature, embedded in paraffin, cut into sections with a thickness of 4 μm and placed on slides. The sections were dewaxed, dehydrated and treated with sodium citrate buffer for antigen repair. The sections were then immersed in a 3% H_2O_2/ethanol solution to inhibit endogenous peroxidases and were then blocked with 3% bovine serum albumin. The sections were incubated overnight at 4°C with the primary antibody (anti-TIGAR antibody; Abcam, ab189164). After washing with PBS (pH 7.4) for 10 min, secondary antibodies (HRP-labelled goat anti-rabbit; Servicebio, No. GB23303) were added, and the sections were incubated for 20 min and reacted with DAB for 1 min. The sections were then restained with haematoxylin before being dehydrated with ethanol and xylene. Each slide was examined microscopically, and three fields of view were randomly selected for observation under a 100× light microscope. Brownish-yellow particles were regarded as indicating positive expression. The cumulative mean OD of the positively stained areas of each section was statistically analysed using Image-Pro Plus 6.0 software to semi-quantitatively determine the level of TIGAR.

We also determined the expression level of TIGAR in human gastric mucosa using the immunoreactivity score (IRS) in the following way: we invited two pathologists to assess the intensity of immunohistochemical (IHC) staining of TIGAR in the human gastric mucosa in a randomized manner using magnifications of 100× and 200× without clinicopathological data. The percentage of positive cells was calculated by IPP software, and the IRS was calculated for the semi-quantitative determination of human TIGAR. The IRS was determined from the sum of the percentage of positive cells (0 points, 0–5%; 1 point, 6–25%; 2 points, 26–50%; 3 points, 51–75%; and 4 points, 76–100%) and the staining intensity score (0 points, no staining; 1 point, weak staining; 2 points, moderate staining; and 3 points, strong staining). A final IRS of >4 indicates strong positive expression, whereas a score of <4 indicates weak positive expression.

2.9 Enzyme-linked immunosorbent assay

According to the instructions of an enzyme-linked immunosorbent assay (ELISA) kit (mlbio, ml202850, ml059197), 20 mg tissue was taken and added to 20 μL PBS before grinding and homogenization at 4°C. After centrifugation at 2000 rpm for 20 min, the supernatant was taken. Blank wells, standard wells and wells for the samples to be tested were set up. The concentrations of the standard in the wells were 8, 4,

2, 1, 0.5 and 0 ng mL^{-1}, respectively. The blank wells were set up without samples or enzyme standard reagent. The standard wells were set up with 50 μL aliquots of the standard with different concentrations. The sample wells were set up with 40 μL sample diluent, followed by 10 μL of the sample to be tested (the final dilution of the sample was thus 5×), which were mixed with gentle shaking. Except for the blank wells, 100 μL enzyme standard reagent was added to each well, mixed with gentle shaking, covered with a plate sticker and incubated at 37°C for 1 h. The liquid in the wells was discarded, and the wells were shaken until dry. A 350 μL aliquot of washing solution was added to each well, allowed to stand for 30 s and then discarded; this process was repeated five times, and the wells were then patted dry. Aliquots of 50 μL chromogenic agent A and 50 μL chromogenic agent B were added to each well, shaken gently and mixed well, and the colour was allowed to develop at 37°C for 15 min. A 50 μL aliquot of terminating solution was added to each well to terminate the reaction. The measurements were zeroed against the blank wells, and the OD of the sample in each well was measured sequentially at 450 nm with an enzyme marker within 15 min of the termination of the reaction. The perigastric tissues were weighed, added to the corresponding amount of PBS and homogenized, and the supernatant was taken for analysis. According to the instructions of the ELISA kit, ELISA Calc software was used to generate the standard curve and calculate the regression equation according to the concentration and OD value of the standard, and the protein contents of the samples to be tested were calculated according to the regression equation.

2.10 Microdetermination

According to the instructions of a GSH assay kit (Hailian Biologicals, m1076450), tissues were first washed twice with PBS, and then a 0.1 g sample was weighed out. Liquid nitrogen was added, and then 1 mL reagent I was added. The mixture was ground rapidly and centrifuged at 8000 rpm for 10 min at 4°C. The supernatant was kept at 4°C to be tested. In the blank tube assay, to a 96-well plate were added 20 μL distilled water, 140 μL reagent II and 40 μL reagent III, which were mixed well. A 1 mg sample of the standard was weighed out and dissolved in 1 mL distilled water to give a concentration of 1 mg mL^{-1}. The resulting solution was taken to prepare the standard with concentrations of 200 μg mL^{-1}, 100 μg mL^{-1}, 50 μg mL^{-1}, 25 μg mL^{-1} and 12.5 μg mL^{-1} (diluted tenfold with reagent I). A 1.5 mL Eppendorf tube was taken, to which 20 μL standard, 140 μL reagent II and 40 μL reagent III were added, mixed and allowed to stand for 2 min. The absorbance at 412 nm was measured, and the absorbance minus that of a blank well (A1) was used as the horizontal coordinate to generate the standard curve of absorbance (x) versus concentration (y, μg mL^{-1}). In the sample tube measurements, to a 96-well plate 20 μL sample, 140 μL reagent II and 40 μL reagent III were added, mixed and left for 2 min. The absorbance at 412 nm (A2) was measured, and ΔA was defined as A2 − A1. The standard curve was generated from the standard concentrations and OD values using ELISA Calc software, and the regression equation was derived, namely, [GSH] = y × volume of supernatant added to the reaction system/(volume of supernatant added to the reaction system/total volume of supernatant × sample mass), from which the GSH concentration was calculated.

2.11 Statistical processing

SPSS 25.0 software was used for statistical analysis. One-way analysis of variance was used to analyse comparisons among groups. Tukey's test was used to compare the mean square deviations for the two groups. When the variance was not uniform, Dunnett's T3 test was used. The data were expressed as the mean ± standard error of the mean. A *P*-value of less than 0.05 was considered to be statistically significant.

3. Results

3.1 Effect of GRg3 on the body weight of rats with GPL

As shown in Fig. 2(A), at week 20 the body weight of rats in the model group was significantly reduced in comparison with the normal group, and the difference was statistically significant ($P < 0.01$). After treatment, the body weight of rats in the folic acid and GRg3 groups was significantly higher in comparison with the model group ($P < 0.01$ and $P < 0.01$), and the high-dose GRg3 group displayed a significant increase in comparison with the folic acid group ($P < 0.01$). The above results indicated that GRg3 could effectively increase the body weight of rats with GPL.

3.2 Effect of GRg3 on the histopathology of the gastric mucosa in rats with GPL

As shown in Fig. 2(B), in the normal group rats had smooth mucosal folds, mucus adhesion on the surface, no erosion or bleeding, uniform thickness of the gastric wall and high elasticity. In the model group rats had rough mucosal folds, low glossiness, reduced mucus adhesion on the surface, dark red tissue colour, thickened blood vessels, scattered bleeding, varying thickness of the gastric wall and reduced elasticity. After continuous treatment for 12 weeks, the gastric mucosal lesions were all alleviated to different degrees.

The degree of damage to the gastric mucosa was determined by histopathological examination. As shown in Fig. 2(C), in comparison with the normal group the model group had incomplete gastric mucosa, a less elastic gastric wall and a different basement membrane thickness. Within the disordered gastric mucosal epithelial tissue, enlarged and dilated glands were seen among the dysplastic gastric epithelial cells. In addition, the gastric mucosal epithelial cells exhibited different morphological sizes and marked heterogeneity, and inflammatory cells had infiltrated mesenchymal cells. The heterogeneous hyperplastic glands were significantly enlarged, irregularly arranged and weakly stained, which suggested a diffuse increase in abnormal heterogeneous hyperplasia in the gastric epithelium in the model group. It is noteworthy that the abnormal proliferation of gastric mucosal epithelial cells in the high-, medium- and low-dose GRg3 groups became less extensive, scattered and confined to the basement membrane side, which suggested that GRg3 had a restorative effect on the gastric mucosa in rats.

We used AB-PAS staining to accurately determine the type of IM. As shown in Fig. 2(D), in the model group the mucinous metaplastic tissue was stained positively by AB-PAS, which indicated that the gastric fundic wall cells and principal cells were replaced by foamy cells containing neutral and acidic mucin. The gastric mucosa was extensive and stained deeply, and the substrate exhibited predominant IM. IM of incomplete cells occurred on the luminal side of the stomach, whereas IM of complete cells occurred in the lamina propria. Interestingly, the dangerous demarcation between GPL and GC, congested tubular gland structures and back-to-back tubular structures were significantly alleviated after treatment with GRg3.

3.3 Effect of GRg3 on apoptosis and ROS levels in rats with GPL

In order to confirm the relationship between apoptosis and the development of GPL, we detected apoptosis by TUNEL staining. After TUNEL staining, the nuclei of normal cells were blue, whereas the nuclei of apoptotic cells were brown.

As shown in Fig. 3(A) and 3(D), significant apoptosis was seen in gastric mucosal epithelial cells in the normal group. Apoptosis in gastric mucosal epithelial cells in the model group was significantly reduced in comparison with the normal group, and the difference was statistically significant ($P < 0.01$). After treatment, the number of apoptotic cells in the folic acid and GRg3 groups was significantly higher in comparison with the model group ($P < 0.01$), and the high-dose GRg3 group displayed a significant increase in comparison with the folic acid group ($P < 0.01$). The above results suggest that GRg3 can effectively increase apoptosis in the gastric mucosal epithelium and inhibit excessive proliferation of gastric mucosal cells, which thus reduces the risk of cell mutation.

We believe that the expression level of ROS is closely associated with apoptosis of gastric mucosal cells. We therefore used the fluorescent probe dihydroethidium to determine the expression level of ROS in the epithelial tissues of the gastric mucosa. As shown in Fig. 3(B) and 3(C), ROS expression was occasionally seen in the gastric mucosal tissues of rats in the normal group. ROS expression in the model group exhibited a significant increase ($P < 0.05$) in comparison with the normal group. The moderate increase in ROS expression could cause the accumulation of large amounts of oxidized proteins and lipids, which would increase the risk of cell mutation and promote the progression of GPL to GC. After treatment, the folic acid and GRg3 groups both displayed a significant increase in ROS content in comparison with the model group ($P < 0.05$), which indicated that GRg3 could promote apoptosis, inhibit abnormal cell proliferation and retard the progression of GPL by increasing the expression level of ROS.

3.4 Regulation of G6PDH, NADP and GSH contents in rats with GPL by GRg3

We believe that increases in G6PDH, NADP and GSH contents may disrupt the original redox balance in cells and thus increase the ROS concentration without triggering apoptosis, and the subsequent rapid proliferation of cells is one of the main reasons for the progression of GPL.

G6PDH is an upstream protein of NADP that can directly affect the level of NADP. The regulatory role of the antioxidant system is particularly critical because the level of ROS in tumour cells is higher than that in normal cells owing to defects in the antioxidant enzyme system and the presence of genetic mutations and is close to the threshold limit that causes cell death. G6PDH is a key protein in the cellular antioxidant system, and therefore the study of the regulatory mechanism of G6PDH has become a current topic of research [27]. We investigated whether GRg3 acts to inhibit the progression of GPL by affecting G6PDH. As shown in Fig. 4(A), the ELISA analysis suggested that the G6PDH content appeared to have increased in the model group in comparison with the normal group ($P < 0.01$), which may indicate that the cells were affected by the upregulation of TIGAR and that the G6PDH content was thus increased. In contrast, the G6PDH contents in the folic acid group and the high- and medium-dose GRg3 groups were significantly lower in comparison with the model group ($P < 0.01$). These findings suggest that GRg3 can effectively downregulate G6PDH.

Similarly, we examined NADP, including $NADP^+$ and NADPH, which are interconvertible. NADP is an important indicator of the activity and amount of G6PDH [28]. NADP is also an essential reducing agent in anabolic processes and is a key factor in the cellular scavenging of ROS. NADP protects mitochondria from damage due to ROS and is also essential for the synthesis of fatty acids, cholesterol and deoxyribonucleotides. As shown in Fig. 4(B), the model group of rats with GPL displayed a significant increase in NADP content in comparison with the normal group ($P < 0.01$), which indicated that the gastric mucosal epithelial cells were affected by TIGAR and G6PDH, which upregulated NADP. The folic acid group exhibited downregulation of NADP in comparison with the model group ($P < 0.01$). There was a downward trend in NADP content in the GRg3 groups in comparison with the model group, but it was not statistically significant, which may have been due to the small sample size. In combination with the above results, this indicated that GRg3 can reduce the level of NADP.

GSH is an antioxidant that plays the role of a free radical scavenger and detoxifying agent in cells [29]. GSH is closely associated with the development of several types of cancer and plays different roles in the early and late stages of cancer [30]. By measuring the level of GSH, we aimed to clarify the role that GSH plays in the progression of GPL to GC and to clarify whether GRg3 plays a role in the treatment of GPL by interfering with GSH.

As shown in Fig. 4(C), the GSH content in tissue from rats in the model group was significantly higher in comparison with that in the normal group ($P < 0.01$). After treatment, the GSH content in tissue from rats in each treatment group decreased to a certain extent in comparison with that in the model group and in the GRg3 groups was statistically significantly lower in comparison with that in the model group ($P < 0.05$).

3.5 TIGAR expression is upregulated in human GPL samples in comparison with normal mucosa samples

TIGAR is a TP53-induced regulator of glycolysis and apoptosis [31, 32]. To determine the pathological role of TIGAR in the progression to GC, we investigated the expression pattern of TIGAR in GC samples using data from the TCGA database. The results are shown in Fig. 5(A), according to which TIGAR expression levels were significantly higher in GC samples in comparison with normal specimens ($P < 0.001$). This result suggests that upregulation of DLL4 may play an important role in the malignant progression of human GC.

In addition, to identify the TIGAR-associated cellular processes and signalling pathways in GC, GSEA was performed using transcriptomics data from the TCGA. The analysis indicated that upregulated TIGAR was enriched in the apoptosis, cytosolic DNA-sensing pathway, nucleotide excision repair, p53 signalling pathway and RNA degradation pathways (Fig. 5(B)).

We studied the expression and staining intensity of TIGAR in 52 normal gastric mucosa specimens and 69 gastric mucosa specimens from patients with GPL (see Table 1). We found that the strong positivity rate for TIGAR was 36.5% (19/52) in normal gastric mucosa specimens, whereas in GPL specimens the strong positivity rate for TIGAR was 58%, and the difference was statistically significant ($P < 0.05$). Interestingly, we found no clear correlations between TIGAR staining intensity and patients' age and gender, the site of sampling and *Helicobacter pylori* infection ($P > 0.05$), and the difference in TIGAR staining intensity between IM and DYS was not significant ($P > 0.05$).

The semi-quantitative determination of TIGAR was performed by calculating the IRS, as shown in Fig. 5(C) and 5(F). It was found that TIGAR expression in gastric mucosa from normal subjects was at a low level, whereas after the development of GPL TIGAR expression appeared to increase. TIGAR expression in both IM and DYS specimens was significantly higher than that in specimens from normal subjects ($P < 0.01$ and $P < 0.05$).

Table 1
Correlation between TIGAR positivity and clinicopathological characteristics of patients with gastric precancerous lesions

Variable	Case	Strong positivity	Weak positivity/ absent	P-value, strong vs weak/absent
Age				
< 60	44	26	18	0.803
≥ 60	25	14	11	
Gender				
Male	34	21	13	0.529
Female	35	19	16	
Location of lesion				
Body	10	5	5	0.907
Angle	13	7	6	
Antrum	34	21	13	
Multiple	12	7	5	
Hp infection				
Negative	28	14	14	0.268
Positive	41	26	15	
Histopathological category				
Normal gastric epithelium	52	19	33	0.020
Gastric precancerous lesions	69	40	29	
Small intestinal-type metaplasia	18	10	8	0.732
Colonic-type metaplasia	16	7	9	
Mild dysplasia	15	8	7	0.409
Moderate dysplasia	12	9	3	
Severe dysplasia	8	6	2	

3.6 Effect of GRg3 on TIGAR expression in rats with GPL

We also examined TIGAR expression in rat gastric mucosa using both IHC and western blotting (WB) assays. As shown in Fig. 5(D) and 5(E), the IHC assay demonstrated that the expression level of TIGAR in gastric mucosal epithelial cells from rats in the model group exhibited an increase in comparison with that in the normal group ($P < 0.05$). After treatment, the expression level of TIGAR in all groups displayed different degrees of downregulation, among which that in the high-dose GRg3 group was statistically significant in comparison with that in the model group ($P < 0.05$).

Similarly, as shown in Fig. 5(G) and 5(H), the WB results confirmed the IHC assay results. The TIGAR expression level appeared to be higher in the model group in comparison with the normal group, and the difference was statistically significant ($P < 0.01$). This indicated that the fact that TIGAR regulates the cellular redox status and induces the overproliferation of gastric mucosal epithelial cells is one of the main factors that lead to the development of GPL. After the intervention, the TIGAR expression level in each GRg3 group displayed a significant decrease in comparison with the model group ($P < 0.01$), which indicated that GRg3 can effectively reduce the TIGAR expression level.

In summary, GRg3 has the effect of regulating ROS, GSH, G6PDH and NADP in rats with GPL, which in turn promotes apoptosis of gastric mucosal epithelial cells, alleviates abnormal changes in the gastric mucosa and reduces the risk of progression of the disease.

4. Discussion

The high mortality and morbidity rates of GC have put enormous pressure on global healthcare systems, and it is therefore important to discover potentially effective treatments for GPL. There is growing evidence that GRg3 plays a role in reducing toxic effects and enhancing the efficacy of treatment when used as an adjuvant in conventional cancer therapy [12]. Previous studies have confirmed that GRg3 can alleviate GPL in mice by inhibiting glycolysis via the PI3K/Akt/miRNA-21 pathway [33]. Via this study, we found that GRg3 could also play a role in inhibiting the progression of GPL by regulating ROS and inducing apoptosis in gastric mucosal epithelial cells.

We used a rat model of GPL induced by MNNG in combination with ammonia in a composite modelling method. By staining with H&E and AB-PAS, we found that the distorted morphology, structural disorder and cellular heteromorphism in the form of epithelial glands and intestinal epithelial metaplastic lesions in the gastric mucosa of rats in the GRg3 groups were alleviated to different degrees. This indicated that GRg3 can effectively inhibit the development of IM and DYS and can effectively prevent malignant transformation of the gastric mucosa in rats with GPL.

ROS plays the role of a ‘double-edged sword’ in the development of cancer. On the one hand, in cancer cells, owing to mitochondrial dysfunction, metabolic alterations and frequent genetic mutations, the concentration of ROS increases significantly, leading to the accumulation of large amounts of oxidized proteins, DNA and lipids, which promote excessive proliferation and metastasis of cancer cells and thus play a role in the development of cancer [34]. On the other hand, when the concentration of ROS exceeds

the threshold value, which triggers irreversible oxidative stress, it can promote apoptosis in tumour cells and thus hinder the development of cancer [35].

In the GPL stage, the ROS content in the model group increased significantly in comparison with the normal group, which would lead to accelerated metabolism and uncontrolled proliferation of gastric mucosal epithelial cells and the gradual progression of the disease. The expression of NADP, G6PDH and GSH decreased after treatment, with downregulation of the upstream factor TIGAR, and the intracellular ROS content in gastric mucosal epithelial cells in each treatment group increased further in comparison with the model group. We then detected apoptosis by TUNEL staining and found that after treatment with GRg3 the apoptosis rate of gastric mucosal epithelial cells increased significantly in comparison with that of the model group, which indicated that GRg3 may induce apoptosis by regulating the expression level of ROS and thus play a role in the inhibition of abnormal cell proliferation to retard the progression of the disease.

TIGAR is a TP53-induced regulator of glycolysis and apoptosis [31, 32]. Recent studies suggest that various cancer tissues, including those in GC, exhibit increased levels of TIGAR and that certain types of cancer are suppressed after knockdown of TIGAR [25, 36, 37].

Our experimental results suggest that TIGAR is highly expressed in GPL in both rat gastric mucosal tissues and human gastric mucosal tissues, which is consistent with the results for TIGAR expression in several types of cancer [36, 38]. However, there are no studies that indicate the role of TIGAR in GPL, and it is therefore of great interest to further investigate the exact role played by TIGAR in the progression of GPL to GC.

The present study found that TIGAR protein expression was significantly higher in the gastric mucosa of rats with GPL and human gastric mucosal epithelial cells in comparison with normal rats, which suggested that overactivation of TIGAR may be one of the main factors that promote carcinogenesis via GPL. However, after treatment with folic acid and GRg3, TIGAR protein expression in rat gastric mucosa was significantly lower in comparison with the model group. This further reduced intracellular expression levels of G6PDH, NADP and GSH, which helped to increase the intracellular ROS concentration to induce apoptosis and thus served to inhibit the abnormal proliferation and differentiation of gastric mucosal epithelial cells and retard the progression of GPL to GC.

Moreover, the present study found that, although there was a decreasing trend in the NADP content after treatment with GRg3, the difference was not statistically significant, which may have been due to the small sample size. It is also possible that NADP is not a target of GRg3 in the treatment of GPL. In addition, GRg3 regulates the cellular redox status as a complex network system. Further experimental investigation is therefore needed to determine the detailed biological mechanism of the regulation of ROS by GRg3.

5. Conclusion

GRg3 was effective in alleviating IM and DYS lesions and retarding the progression of the disease in rats with GPL. Overexpression of TIGAR, NADP, GSH and G6PDH in the gastric mucosal epithelium of rats with GPL, which may be one of the causes of the increase in ROS content, is an important molecular event in the progression of GPL. After treatment with GRg3, as the expression of TIGAR, NADP, GSH and G6PDH decreased, the intracellular ROS concentration further increased, which in turn induced apoptosis and served to inhibit the abnormal proliferation and differentiation of gastric mucosal epithelial cells and retard the progression of GPL to GC.

Our study suggests that an abnormal redox status and proliferative state of gastric mucosal epithelial cells exist during the developmental stage of GPL. Whereas GRg3 induced apoptosis and inhibited abnormal proliferation of gastric mucosal epithelial cells, the mechanism may be related to downregulation of TIGAR, NADP, GSH, and G6PDH in gastric mucosal epithelial cells and an increase in ROS concentration in rats with GPL. These findings provide experimental evidence for the potential use of GRg3 as a drug for the treatment of GPL. Meanwhile in future research, we can combine the pathogenesis theory [39] of traditional Chinese medicine to find more traditional Chinese medicine with a therapeutic effect on GPL.

Abbreviations

Ginsenoside Rg3: GRg3; gastric precancerous lesion: GPL; N-methyl-N'-nitro-N-nitrosoguanidine: MNNG; reactive oxygen species: ROS; TP53-induced glycolysis and apoptosis regulator: TIGAR; nicotinamide adenine dinucleotide phosphate: NADP; glucose-6-phosphate dehydrogenase: G6PDH; glutathione: GSH; intestinal metaplasia: IM gastric epithelial dysplasia: DYS; gastric cancer: GC; p-phosphoinositide 3-kinase: PI3K; haematoxylin and eosin: H&E; Alcian blue–periodic acid Schiff: AB-PAS; transferase dUTP nick end labelling: TUNEL; phosphate-buffered saline: PBS; Streptavidin–horseradish peroxidase: HRP; Tris-buffered saline–Tween-20: TBST; the Cancer Genome Atlas: TCGA; gene set enrichment analysis: GSEA; immunoreactivity score: IRS; immunohistochemical: IHC; enzyme-linked immunosorbent assay: ELISA western blotting: WB.

Declarations

Acknowledgements

The authors would like to thank all of the teachers and classmates who contributed to this study.

Authors' contributions

JHZ and WHL designed the study. SBL, ZLL and JC carried out the experiments. GM and YC interpreted the results of the experiments. YC, TX AND DYG organized the database and conducted the statistical analysis. SBL, GM and XDC prepared the manuscript. WHL and JHZ confirmed the authenticity of all the raw data. All authors have read and approved the final version of the manuscript.

Funding

This work was supported by the National Natural Science Foundation of China (grant nos. 81804066, 82174346 and 81904178), and by Xinglin Scholar Research Promotion Project of Chengdu University of TCM (grant nos. QNXZ2019017 and QNXZ2020003) and “Hundred Talents Program” of the Hospital of Chengdu University of Traditional Chinese Medicine (grant nos. 21-Y17) and Project of Sichuan Administration of traditional Chi- nese Medicine (grant no. 2021MS104).

Availability of data and materials

The datasets used and/or analyzed during the current study are available from the corresponding author on reasonable request.

Ethics approval and consent to participate

The animal experiments in this study were conducted according to the Guidelines for the Care and Use of Laboratory Animals, and were approved by Chengdu University of Traditional Chinese Medicine (audit filing number: 2019-17), and carried out in compliance with the ARRIVE guidelines.

Consent for publication

Not applicable.

Competing interests

The authors declare no conflicts of interest in this work.

Author details

[1]Basic Medical College, Chengdu University of Traditional Chinese Medicine, Chengdu, China,[2]Department of Surgery, Sichuan Cancer Hospital, School of Medicine, University of Electronic Science and Technology of China, Chengdu, China, [3] Hospital of Chengdu University of Traditional Chinese Medicine, Chengdu, China,[4] Department of Chinese Internal Medicine, Hospital of Chengdu University of Traditional Chinese Medicine, Chengdu, China,[5] TCM Regulating Metabolic Diseases Key Laboratory of Sichuan Province, Hospital of Chengdu University of Traditional Chinese Medicine, Chengdu, China

References

1. Sung, H., J. Ferlay, R.L. Siegel, et al., Global cancer statistics 2020: GLOBOCAN estimates of incidence and mortality worldwide for 36 cancers in 185 countries. CA Cancer J Clin, 2021.
2. Rugge, M., K. Sugano, C. Scarpignato, et al., Gastric cancer prevention targeted on risk assessment: Gastritis OLGA staging. Helicobacter, 2019. 24(2): e12571.

3. Srivastava, A.,G.Y. Lauwers, Gastric epithelial dysplasia: the Western perspective. Dig Liver Dis, 2008. 40(8): 641–9.
4. Tu, C., B. Wan, Y. Zeng, Ginsenoside Rg3 alleviates inflammation in a rat model of myocardial infarction via the SIRT1/NF-kappaB pathway. Exp Ther Med, 2020. 20(6): 238.
5. Liu, X., Z. Zhang, J. Liu, et al., Ginsenoside Rg3 improves cyclophosphamide-induced immunocompetence in Balb/c mice. Int Immunopharmacol, 2019. 72: 98–111.
6. Nakhjavani, M., E. Smith, A.R. Townsend, et al., Anti-Angiogenic Properties of Ginsenoside Rg3. Molecules, 2020. 25(21).
7. Kwok, H.H., G.L. Guo, J.K. Lau, et al., Stereoisomers ginsenosides-20(S)-Rg(3) and -20(R)-Rg(3) differentially induce angiogenesis through peroxisome proliferator-activated receptor-gamma. Biochem Pharmacol, 2012. 83(7): 893–902.
8. Gum, S.I.,M.K. Cho, The amelioration of N-acetyl-p-benzoquinone imine toxicity by ginsenoside Rg3: the role of Nrf2-mediated detoxification and Mrp1/Mrp3 transports. Oxid Med Cell Longev, 2013. 2013: 957947.
9. Yu, Y., C. Zhang, L. Liu, et al., Hepatic arterial administration of ginsenoside Rg3 and transcatheter arterial embolization for the treatment of VX2 liver carcinomas. Exp Ther Med, 2013. 5(3): 761–766.
10. Park, H.M., S.J. Kim, J.S. Kim, et al., Reactive oxygen species mediated ginsenoside Rg3- and Rh2-induced apoptosis in hepatoma cells through mitochondrial signaling pathways. Food Chem Toxicol, 2012. 50(8): 2736–41.
11. Joo, E.J., J. Chun, Y.W. Ha, et al., Novel roles of ginsenoside Rg3 in apoptosis through downregulation of epidermal growth factor receptor. Chem Biol Interact, 2015. 233: 25–34.
12. Sun, M., Y. Ye, L. Xiao, et al., Anticancer effects of ginsenoside Rg3 (Review). Int J Mol Med, 2017. 39(3): 507–518.
13. Yang, Q., N. Cai, D. Che, et al., Ginsenoside Rg3 inhibits the biological activity of SGC-7901. Food Sci Nutr, 2020. 8(8): 4151–4158.
14. Li, B., G. Qu, Inhibition of the hypoxia-induced factor-1alpha and vascular endothelial growth factor expression through ginsenoside Rg3 in human gastric cancer cells. J Cancer Res Ther, 2019. 15(7): 1642–1646.
15. Tao, H., M. Yao, S. Zou, et al., [Effect of angiogenesis inhibitor Rg3 on the growth and metastasis of gastric cancer in SCID mice]. Zhonghua Wai Ke Za Zhi, 2002. 40(8): 606–8.
16. Aziz, F., X. Wang, J. Liu, et al., Ginsenoside Rg3 induces FUT4-mediated apoptosis in H. pylori CagA-treated gastric cancer cells by regulating SP1 and HSF1 expressions. Toxicol In Vitro, 2016. 31: 158–66.
17. Wei, G.H.,X. Wang, lncRNA MEG3 inhibit proliferation and metastasis of gastric cancer via p53 signaling pathway. Eur Rev Med Pharmacol Sci, 2017. 21(17): 3850–3856.
18. Shigenaga, M.K., T.M. Hagen, B.N. Ames, Oxidative damage and mitochondrial decay in aging. Proc Natl Acad Sci U S A, 1994. 91(23): 10771–8.

19. Pelicano, H., D. Carney, P. Huang, ROS stress in cancer cells and therapeutic implications. Drug Resist Updat, 2004. 7(2): 97–110.
20. Ramsey, M.R.,N.E. Sharpless, ROS as a tumour suppressor? Nat Cell Biol, 2006. 8(11): 1213–5.
21. Bradshaw, P.C., Cytoplasmic and Mitochondrial NADPH-Coupled Redox Systems in the Regulation of Aging. Nutrients, 2019. 11(3).
22. Patra, K.C.,N. Hay, The pentose phosphate pathway and cancer. Trends Biochem Sci, 2014. 39(8): 347–54.
23. Cai, T., Y. Kuang, C. Zhang, et al., Glucose-6-phosphate dehydrogenase and NADPH oxidase 4 control STAT3 activity in melanoma cells through a pathway involving reactive oxygen species, c-SRC and SHP2. Am J Cancer Res, 2015. 5(5): 1610–20.
24. Cairns, R.A., I.S. Harris, T.W. Mak, Regulation of cancer cell metabolism. Nat Rev Cancer, 2011. 11(2): 85–95.
25. Liu, Z., Y. Wu, Y. Zhang, et al., TIGAR Promotes Tumorigenesis and Protects Tumor Cells From Oxidative and Metabolic Stresses in Gastric Cancer. Front Oncol, 2019. 9: 1258.
26. Chen Ze-Hui, Wei Yue, Quiet, et al. A literature study on the modelling method of chronic atrophic gastritis and gastric precancerous lesions in rats [J]. Tianjin Chinese Medicine, 2019, 36 (09): 850–855
27. Rao, X., X. Duan, W. Mao, et al., O-GlcNAcylation of G6PD promotes the pentose phosphate pathway and tumor growth. Nat Commun, 2015. 6: 8468.
28. Di Stefano, G., M. Manerba, M. Vettraino, NAD metabolism and functions: a common therapeutic target for neoplastic, metabolic and neurodegenerative diseases. Curr Top Med Chem, 2013. 13(23): 2918–29.
29. Zhang, Z.Z., E.E. Lee, J. Sudderth, et al., Glutathione Depletion, Pentose Phosphate Pathway Activation, and Hemolysis in Erythrocytes Protecting Cancer Cells from Vitamin C-induced Oxidative Stress. J Biol Chem, 2016. 291(44): 22861–22867.
30. Assi, M., The differential role of reactive oxygen species in early and late stages of cancer. Am J Physiol Regul Integr Comp Physiol, 2017. 313(6): R646-R653.
31. Pena-Rico, M.A., M.N. Calvo-Vidal, R. Villalonga-Planells, et al., TP53 induced glycolysis and apoptosis regulator (TIGAR) knockdown results in radiosensitization of glioma cells. Radiother Oncol, 2011. 101(1): 132–9.
32. Bensaad, K., A. Tsuruta, M.A. Selak, et al., TIGAR, a p53-inducible regulator of glycolysis and apoptosis. Cell, 2006. 126(1): 107–20.
33. Liu, W., H.F. Pan, L.J. Yang, et al., Panax ginseng C.A. Meyer (Rg3) Ameliorates Gastric Precancerous Lesions in Atp4a(-/-) Mice via Inhibition of Glycolysis through PI3K/AKT/miRNA-21 Pathway. Evid Based Complement Alternat Med, 2020. 2020: 2672648.
34. Demple, B.,L. Harrison, Repair of oxidative damage to DNA: enzymology and biology. Annu Rev Biochem, 1994. 63: 915–48.

35. Wang, J.,J. Yi, Cancer cell killing via ROS: to increase or decrease, that is the question. Cancer Biol Ther, 2008. 7(12): 1875–84.
36. Wong, E.Y., S.C. Wong, C.M. Chan, et al., TP53-induced glycolysis and apoptosis regulator promotes proliferation and invasiveness of nasopharyngeal carcinoma cells. Oncol Lett, 2015. 9(2): 569–574.
37. Won, K.Y., S.J. Lim, G.Y. Kim, et al., Regulatory role of p53 in cancer metabolism via SCO2 and TIGAR in human breast cancer. Hum Pathol, 2012. 43(2): 221–8.
38. Wanka, C., J.P. Steinbach, J. Rieger, Tp53-induced glycolysis and apoptosis regulator (TIGAR) protects glioma cells from starvation-induced cell death by up-regulating respiration and improving cellular redox homeostasis. J Biol Chem, 2012. 287(40):33436–46.
39. Xu Q, Guo Q, Wang C X, et al. Network differentiation: A computational method of pathogenesis diagnosis in traditional Chinese medicine based on systems science[J]. Artificial Intelligence in Medicine, 2021(7724):102134.

Figures

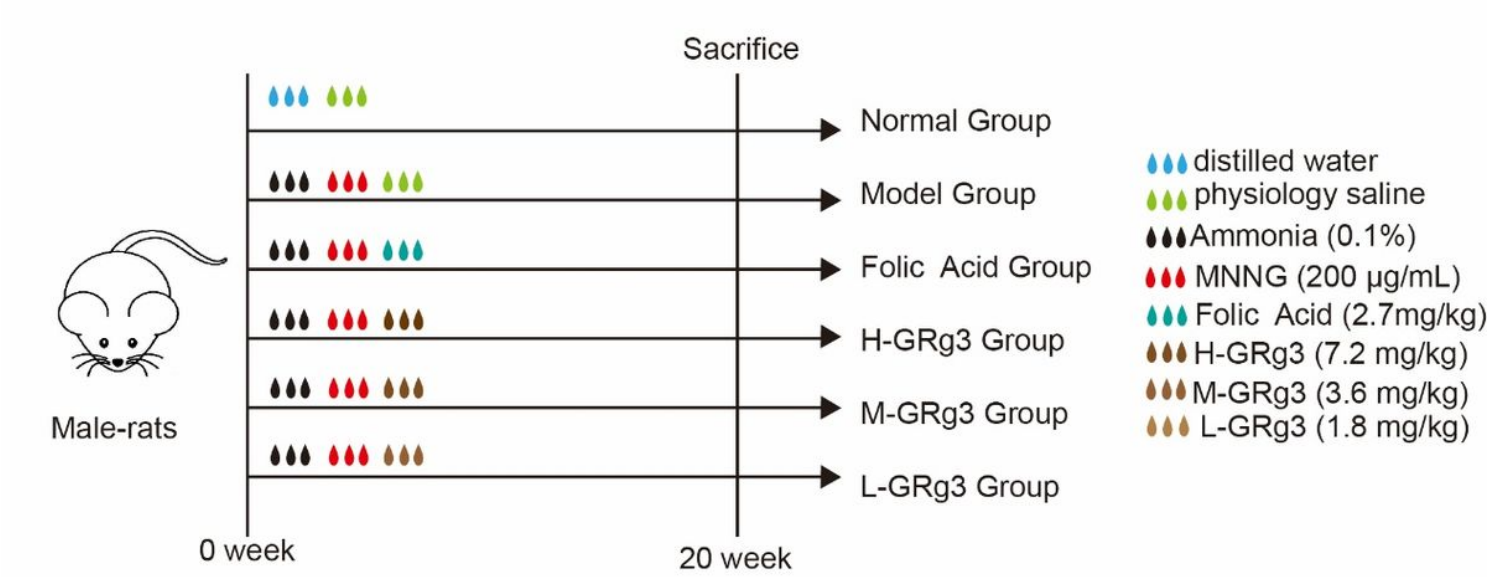

Figure 1

Scheme of the experimental design (n = 12 rats per group).

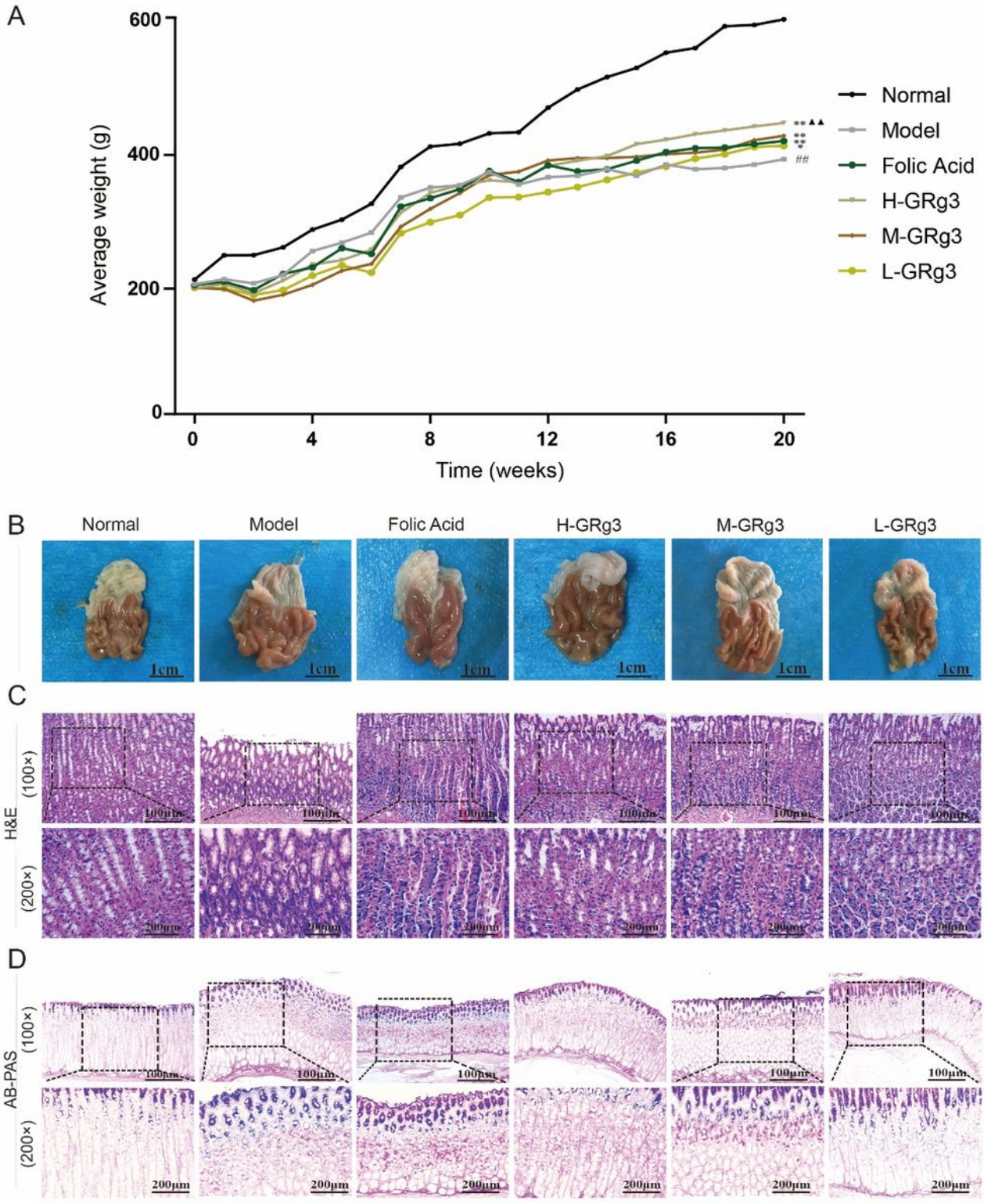

Figure 2

Effect of GRg3 on the body weight and histopathology of the gastric mucosa in MNNG-induced GPL rats. (A) Observations of gastric mucosa from rats with gastric precancerous lesion. (B) Histopathological changes in gastric mucosa from rats in various groups (haematoxylin and eosin staining, 100× and 200× magnification). (C) Integrity of gastric mucosa from rats in various groups (Alcian blue–periodic acid Schiff staining, 100× and 200× magnification). The body weight in the 20th week results are expressed

as the mean ± SEM (n = 10 for each group). #P < 0.05, ##P < 0.01 vs normal group; *P < 0.05, **P < 0.01 vs model group; ▲P < 0.05, ▲▲P < 0.01 vs folic acid group.

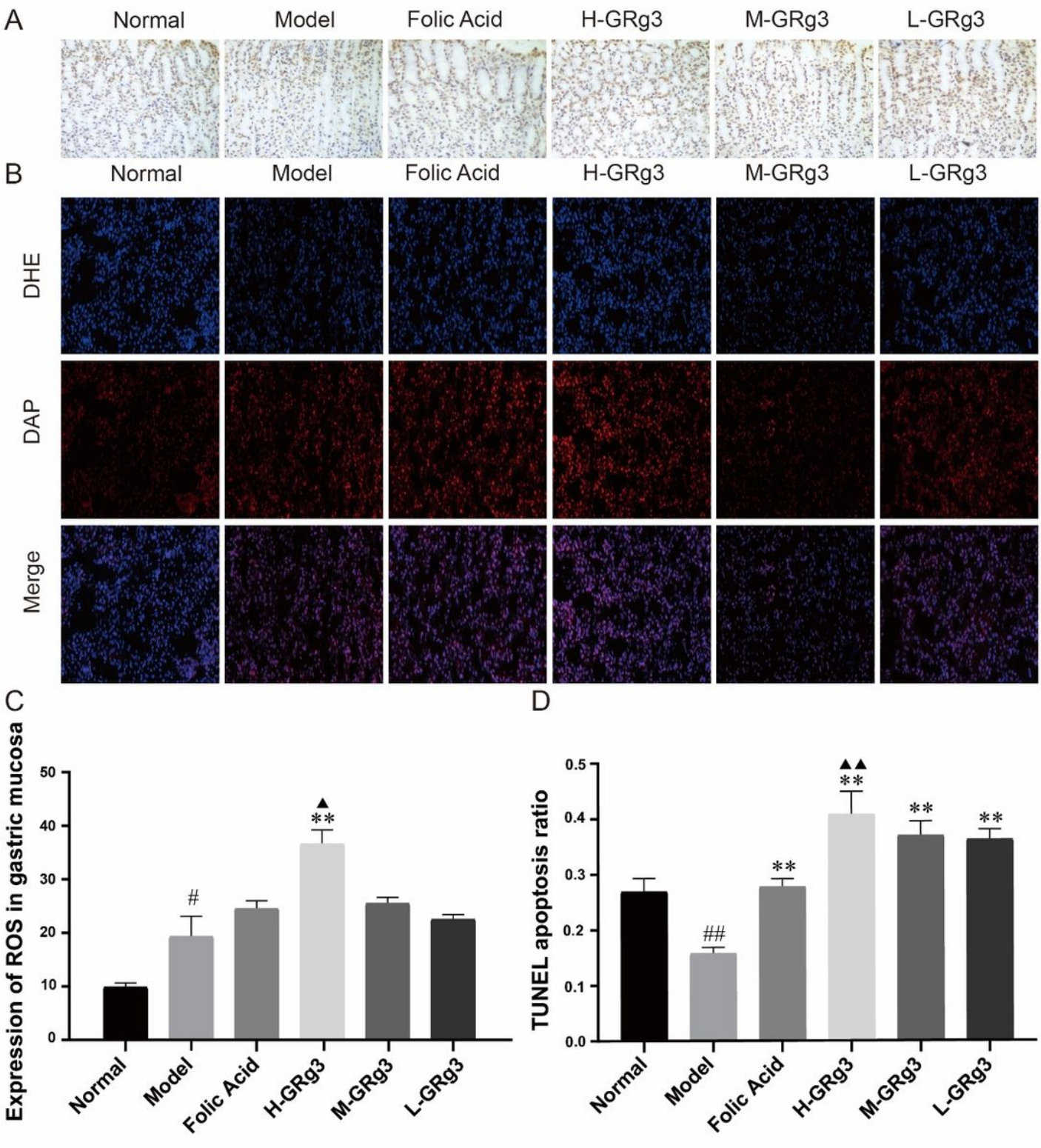

Figure 3

Effects of GRg3 on the expression levels of apoptosis and ROS in in MNNG-induced GPL rats. (A) Apoptosis in gastric mucosa from rats in various groups shown by terminal deoxynucleotidyl transferase dUTP nick end labelling (TUNEL) staining (400× magnification). (B) Effect of GRg3 on ROS in gastric

mucosa (40× magnification). (C) Expression of ROS in gastric mucosa. The results are expressed as the mean ± standard error of the mean (SEM) (n = 10 for each group). (D) Apoptosis ratio shown by TUNEL staining. The results are expressed as the mean ± SEM (n = 10 for each group). #P < 0.05, ##P < 0.01 vs normal group; *P < 0.05, **P < 0.01 vs model group; ▲P < 0.05, ▲▲P < 0.01 vs folic acid group.

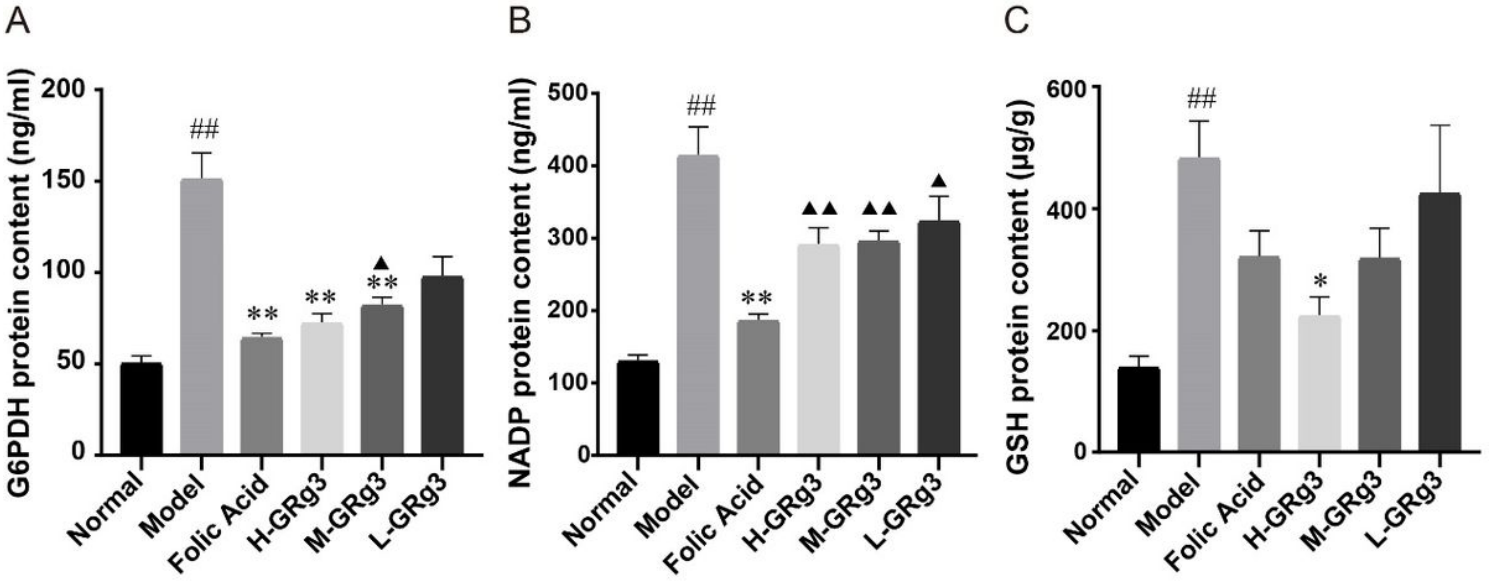

Figure 4

Effects of GRg3 on the expression levels of G6PDH, NADP, GSH in MNNG-induced GPL rats. (A) Effect of GRg3 on expression of glucose-6-phosphate dehydrogenase in gastric mucosa. (B) Effect of GRg3 on expression of nicotinamide adenine dinucleotide phosphate in gastric mucosa. (C) Effect of GRg3 on expression of glutathione in gastric mucosa. The results are expressed as the mean ± SEM (n = 10 for each group). #P < 0.05, ##P < 0.01 vs normal group; *P < 0.05, **P < 0.01 vs model group; ▲P < 0.05, ▲▲P < 0.01 vs folic acid group.

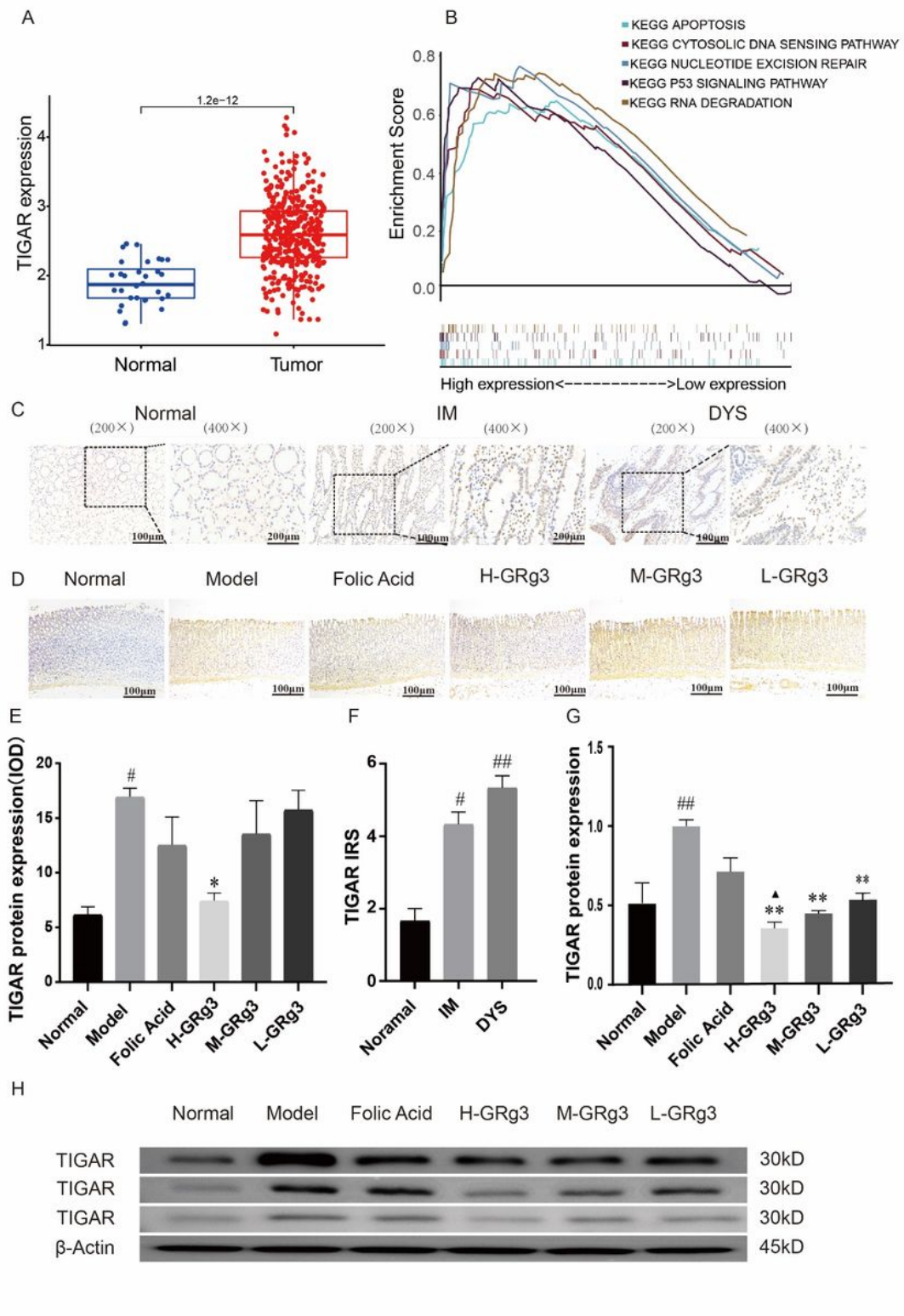

Figure 5

TIGAR expression is up-regulated in human GPL samples than in normal mucosa samples, and GRg3 can effectively reduce the TIGAR expression level in MNNG-induced GPL rats. (A) Expression of TP53-induced glycolysis and apoptosis regulator (TIGAR) in gastric cancer from data retrieved from the Cancer Genome Atlas database. (B) Results of enrichment analysis of a TIGAR gene set. (C) Determination of TIGAR in human gastric mucosa samples from various groups by an immunohistochemistry (IHC) assay (200×

and 400× magnification). (D) Determination of TIGAR in rat gastric mucosa samples from various groups by an IHC assay (100× magnification). (E) TIGAR protein expression determined from cumulative mean optical density. The results are expressed as the mean ± SEM (n = 10). (F) TIGAR protein expression in human gastric mucosa determined from the immunoreactivity score. The results are expressed as the mean ± SEM (n = 10). (G) TIGAR protein expression determined by western blotting (WB). The results are expressed as the mean ± SEM (n = 3). (H) Determination of TIGAR in rat gastric mucosa from various groups by WB. #P < 0.05, ##P < 0.01 vs normal group; *P < 0.05, **P < 0.01 vs model group; ▲P < 0.05, ▲▲P < 0.01 vs folic acid group.

Supplementary Files

This is a list of supplementary files associated with this preprint. Click to download.

- 1.tif
- 2.tif